

Finite-Momentum Pairing State in Unconventional Rashba Systems

Ran Wang,^{1,2} Song-Bo Zhang,^{3,4} and Ning Hao^{1,2,*}

¹Anhui Province Key Laboratory of Low-Energy Quantum Materials and Devices, High Magnetic Field Laboratory, HFIPS, Chinese Academy of Sciences, Hefei, Anhui 230031, China

²Science Island Branch of Graduate School, University of Science and Technology of China, Hefei, Anhui 230026, China

³Hefei National Laboratory, Hefei, Anhui, 230088, China

⁴International Center for Quantum Design of Functional Materials (ICQD), University of Science and Technology of China, Hefei, Anhui 230026, China

In systems with unconventional Rashba bands, we propose that a finite-momentum pairing state can emerge without the need for an external magnetic field. We analyze the phase transition from a zero-momentum Bardeen-Cooper-Schrieffer (BCS) state to a finite-momentum pairing state using a microscopic interaction model. We demonstrate that the coexistence of zero-momentum and Larkin-Ovchinnikov (LO)-type pairings in different channels provides a well understanding of recent experimental observations of pair-density-wave (PDW) states. Furthermore, we propose that an s-wave BCS superconductor-unconventional Rashba metal (SC-URM) junction can generate an LO-type pairing state via an orbital-selective proximity effect. This nontrivial state can be detected by measuring the Josephson current in an SC-URM-SC junction or through Josephson scanning tunneling microscopy/spectroscopy (JSTM/S). Our results reveal that the internal multi-orbital degrees of freedom play a crucial role in facilitating finite-momentum pairing states.

Introduction.— Finite-momentum pairing states [1, 2] deviate from the conventional BCS state, in which Cooper pairs have zero total momentum. In these unconventional states, Cooper pairs acquire a finite center-of-mass momentum, resulting in spatially modulated superconducting order parameters. Two prominent examples of such states are the Fulde-Ferrell-Larkin-Ovchinnikov (FFLO) state [3–5] and the PDW state [6–13]. In both cases, the superconducting order parameter varies periodically in space, though with different characteristic wavelengths. This difference arises from distinct underlying mechanisms. The FFLO state, first proposed in the 1960s, occurs in systems with Zeeman splitting under an external magnetic field and has recently been suggested to arise in systems with more general time-reversal-symmetry-breaking effects, such as altermagnets [14–17] and flat-band systems [18]. These systems typically feature an imbalance between spin-up and spin-down electron populations or mismatched Fermi surfaces, leading to a tendency for the formation of an FFLO state. The finite momentum corresponds to the imbalanced or mismatched Fermi vector, as illustrated in Fig. 1(a). However, the FFLO state is often difficult to stabilize due to its sensitivity to impurities [19, 20] and the orbital pair-breaking effect of the magnetic field [21, 22]. In contrast, the PDW state does not require an external magnetic field, but it can coexist with or compete against other ordered states, such as charge or spin density waves, as shown in Fig. 1(b). Systems exhibiting PDW states often have strong electronic correlations, such as high-temperature superconductors [6–13] and flat-band systems [23–25]. The complexity of these interactions makes the underlying mechanism of the PDW state a subject of ongoing debate [2, 7, 26].

Rashba spin-orbit coupling (RSOC) plays a fascinat-

ing role in the study of finite-momentum pairing states [5, 27–30]. RSOC arises from structural inversion asymmetry and results in a momentum-dependent splitting of spin bands [31–34], which can profoundly impact the nature of superconducting pairing [35, 36]. Recently, multi-orbital degrees of freedom have been introduced and emphasized in RSOC systems [37, 38], leading to unconventional Rashba bands with anomalous spin textures. These unconventional Rashba systems can host exotic quantum phases and phenomena, both in superconductivity [39] and in spintronics [37, 38, 40, 41].

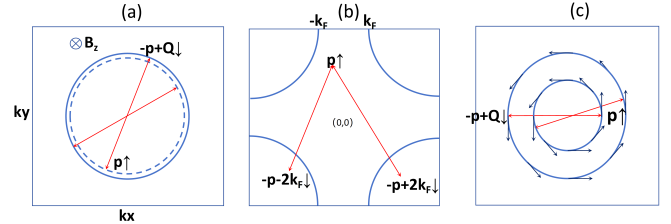


FIG. 1. Schematic of three types of finite-momentum pairing states. (a) The FFLO state driven by an external magnetic field. (b) The PDW state with Amperean pairing in cuprates [11]. (c) The finite-momentum pairing state in unconventional Rashba systems with anomalous spin textures.

In this work, we explore the theoretical framework and propose an experimental scheme for finite-momentum pairing in unconventional Rashba systems, focusing on the conditions necessary for the emergence of such states and the potential experimental signatures that could confirm their existence. Unlike conventional FFLO states, finite-momentum pairing can arise in unconventional Rashba systems without the need for an external field. We begin by analyzing the phase transition from a BCS

state to a finite-momentum pairing state using a microscopic interaction model. Our findings highlight the critical role of internal multi-orbital degrees of freedom in generating intrinsic finite-momentum states. Additionally, we show that the coexistence of zero-momentum and LO-type pairings in different channels provides a comprehensive explanation of recent experimental observations of PDW states. Furthermore, we demonstrate that LO-type pairing can be induced in an URM via an orbital-selective proximity effect and propose detecting this state through measurements of Josephson current in an SC-URM-SC junction or by employing JSTM/S.

Model and pairing symmetry.— To describe the bands of URM [37, 39], we start with a 4×4 Hamiltonian defined in the basis $\hat{c}_{\mathbf{k}}^{\dagger} = (c_{\mathbf{k},1\uparrow}^{\dagger}, c_{\mathbf{k},1\downarrow}^{\dagger}, c_{\mathbf{k},2\uparrow}^{\dagger}, c_{\mathbf{k},2\downarrow}^{\dagger})$,

$$\hat{H}^{UR}(\mathbf{k}) = \xi_{\mathbf{k}} \sigma^0 \tau^0 - \lambda_R (k_y \sigma^1 - k_x \sigma^2) (\tau^0 + \varepsilon \tau^1) + \lambda \sigma^3 \tau^2. \quad (1)$$

Here, $i \in \{1, 2\}$ denotes the effective orbitals, and $\sigma \in \{\uparrow, \downarrow\}$ represents the spin in the electron annihilation operator $c_{\mathbf{k},i\sigma}$. The Pauli matrices $(\sigma^0, \boldsymbol{\sigma})$ and $(\tau^0, \boldsymbol{\tau})$ span the spin and orbital spaces, respectively. $\xi_{\mathbf{k}} = \gamma_0 k^2 - \mu_0$, where γ_0 controls the band curvature near the Fermi surface, and μ_0 is the chemical potential. For convenience, we rescale the chemical potential as $\mu = \mu_0 + \lambda$. λ_R represents the strength of RSOC, while λ denotes the strength of on-site SOC. ε scales the relative strength of inter-orbital RSOC. The energy dispersion of (1) is $E_{\alpha\beta} = \xi_{\mathbf{k}} + \alpha \sqrt{\lambda^2 + \lambda_R^2 k^2} + \beta \varepsilon \lambda_R k$, where $\alpha, \beta \in \{+, -\}$ labels the band indices. When the chemical potential lies within the band gap at $k = 0$, the two Fermi surfaces corresponding to the lower two bands share the same spin chirality, forming the unconventional Rashba bands, as illustrated in Figs. 1(c) and 2(a).

The classification of possible superconducting pairings has been previously established [39]. Here, we focus on pairings arising from widely-used on-site attractive interactions, summarized in Table I. In systems with C_{4v} symmetry, the 1g1 and 1g2 pairings belong to the A_1 irreducible representation (IR), while the 1u pairing belongs to the A_2 IR. These IRs indicate whether coupling occurs between different pairing channels, consistent with our explicit calculations.

Intrinsic finite-momentum pairing.— Since we are interested in finite-momentum pairings, there should be a significant splitting between the lower two bands. To achieve this, we relax the approximation ($\lambda_R k_F / \lambda \ll 1$) used in our previous work [39]. To make the model tractable, we consider the case where $\lambda_R k_F / \lambda < 1$ but not too small. Intuitively, the mismatched concentric Fermi circles may induce finite-momentum Cooper pairs, akin to the magnetic-field-induced FFLO state, as illustrated in Fig. 1(a) and 1(c).

Next, we explore the possibility of finite-momentum pairing using a phenomenological theory of unconventional superconductivity [42–47]. The microscopic

TABLE I. Possible IRs of superconducting pairings in URM under the constraints of group C_{4v} and on-site attractive interactions.

Label	IRs for C_{4v}	Pairing form $\hat{\Gamma}$
1g1	A_1	$i\sigma^2 \tau^0$
1g2	A_1	$i\sigma^2 \tau^1$
1u	A_2	$i\sigma^2 \tau^3$

Hamiltonian is given by $H_{SC} = H_{UR} + H_{int}$, where

$$H_{UR} = \sum_{\mathbf{k}} \hat{c}_{\mathbf{k}}^{\dagger} \hat{H}^{UR}(\mathbf{k}) \hat{c}_{\mathbf{k}}. \quad (2)$$

$$H_{int} = -\frac{1}{2} \sum_{\mathbf{k}, \mathbf{k}', \Gamma, q} v_{\Gamma} \hat{c}_{\mathbf{k}}^{\dagger} \hat{\Gamma} \hat{c}_{-\mathbf{k}+\mathbf{q}}^* \hat{c}_{-\mathbf{k}'+\mathbf{q}}^T \hat{\Gamma}^{\dagger} \hat{c}_{\mathbf{k}'}. \quad (3)$$

Here, $\Gamma \in \{1g1, 1g2, 1u\}$, and v_{Γ} takes constant values. For simplicity, we search for states with $\mathbf{q}_{\mathbf{k}} = q_0 \hat{\mathbf{k}}$. From the linearized gap equations near the superconducting transition temperature T_c , we find that zero-momentum Cooper pairs are always favored in the 1g1 and 1g2 states [48]. However, in the 1u state, finite-momentum pairing ($q_0 = \varepsilon \lambda_R / \gamma'_0$) can be favored if the band splitting is sufficiently large under the condition $q_0/k_0 > (\gamma'_0 k_0^2 / 2 / \pi k_B T_c)^{-1} / a_0$ with $a_0 \approx 3.3$, $\gamma'_0 = \gamma_0 - \lambda_R^2 / (2\lambda)$. Otherwise, the trivial zero-momentum pairing is preferred. Note that $q_0 \equiv k_{out} - k_{in} = \varepsilon \lambda_R / \gamma'_0$, $k_0 \equiv k_{out} + k_{in} = D_0 / \gamma'_0$ with $D_0 = \sqrt{\varepsilon^2 \lambda_R^2 + 4\gamma'_0 \mu}$, $k_{in(out)} \approx (D_0 - (+)\varepsilon \lambda_R) / 2\gamma'_0$. The transition between finite- and zero-momentum pairing is determined by the superconducting susceptibility χ_{1u} as a function of q under different parameters, as shown in Fig. 2 (b) and (c). The peaks of χ_{1u} indicates the presence of superconductivity therein.

The finite-momentum pairing here differs from the FFLO pairing, which has a well-defined center-of-mass momentum \mathbf{q}_0 for Cooper pairs [2, 49, 50]. However, due to C_{4v} symmetry, only four independent \mathbf{q}_0 directions remain. This symmetry allows for a variety of finite-momentum pairings, such as FF-type, LO-type, bidirectional, or double-helix pairings [9]. In practice, perturbations that break the C_4 rotational symmetry make the LO-type pairing the most likely. Figure 2 (d) and 2(e) show the quasi-particle spectrum and spectral function for a superconducting state with pure LO-type pairing, revealing broken particle-hole symmetry and a pair of residual Bogoliubov quasi-particle nodal points.

Implication to experiments.— Recent experiments have reported signatures of PDW orders in monolayer Fe(Te,Se), EuRbFe₄As₄ and UTe₂ [51–56]. Seizing the multi-orbital and inversion-symmetry-breaking characteristics of the systems, our findings may provide a comprehensive understanding of the phenomena observed in the iron-based systems. Specifically, our calculations reveal that the superconducting susceptibility for the 1g1

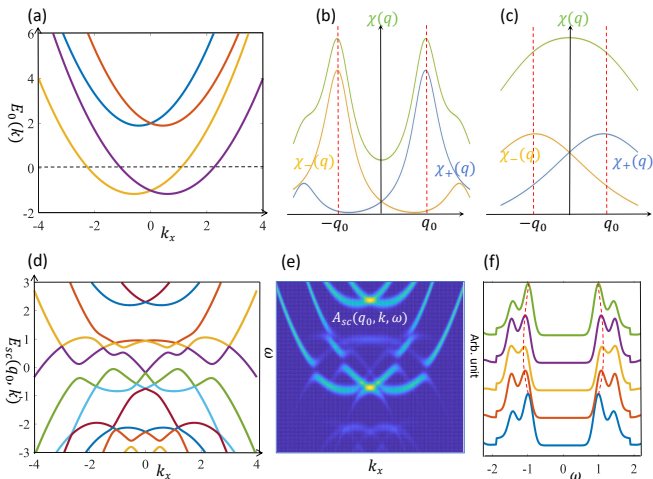


FIG. 2. (a) Band structures of the unconventional Rashba system. The relevant Fermi circles are shown in Fig. 1(c). (b) and (c) Two types of superconducting susceptibility χ_{1u} in $1u$ channel under different λ_R . $\lambda_R=0.5$ in (b) and $\lambda_R=0.1$ in (c). Other parameters in (b) and (c) are $\gamma_0=0.5$, $\mu = 1$, $\lambda=1.5$, $\lambda_R=0.5$, $\varepsilon=1$, and $1/k_B T_c=5$. (d) Energy dispersion of quasi-particle for pure $1u$ LO-type state. The strength of order parameter is $\Delta_{1u}=0.5$. (e) The spectral function corresponding to (d). (f) The density of states of quasi-particle spectrum for the coexistence of both zero-momentum $1g1$ pairing and LO-type $1u$ pairing. The strengths of order parameters are $\Delta_{1g1}=1$ and $\Delta_{1u}=0.5$. In (d)-(f), other parameters are the same as those in (b).

pairing is significantly stronger than that of the $1u$ pairing, with the latter suppressed by a factor of $(\lambda_R k_F / \lambda)^2$ [48]. This suggests that $1g1$ pairing is dominant, while the LO-type $1u$ pairing plays a secondary role when the pairing interactions in both channels are comparable. Importantly, the coexistence of both $1g1$ and LO-type $1u$ pairings can explain the experimentally observed spatial modulation in superconducting order parameter, as shown in Fig. 2(f). The effective superconducting gap can be expressed as $\tilde{\Delta}_0 + \tilde{\Delta}_1 \cos(\tilde{\mathbf{Q}} \cdot \mathbf{r})$, where $\tilde{\mathbf{Q}} = 2\mathbf{q}_0$, owing to the orthogonality of the $1g1$ and $1u$ channels. This explains the experimentally observed short-period spatial modulation or large $\tilde{\mathbf{Q}}$ of the superconducting gap due to the doubled center-of-mass momentum \mathbf{q}_0 here. The temperature evolution of the PDW state observed in $\text{EuRbFe}_4\text{As}_4$ can be explained due to the weaker LO-type $1u$ pairing relative to the $1g1$ pairing. As the temperature rises, the mixed state involving zero-momentum $1g1$ and LO-type $1u$ pairing gradually transitions into a uniform superconducting state with either both zero-momentum $1g1$ and $1u$ pairings or pure zero-momentum $1g1$ pairing. The impact of temperature effect on $1u$ pairing is shown in SMs [48]. Furthermore, under an external magnetic field, the PDW order is suppressed within the vortex halo due to pair-breaking effects on both zero-momentum $1g1$

and LO-type $1u$ pairings from the magnetic field. However, the PDW order persists outside the vortex halo, where the effective magnetic field vanishes.

Extrinsic LO-pairing from proximity effect.— The coexistence of $1g1$ and finite-momentum $1u$ pairings imposes restrictions on the pairing interactions, especially when these interactions differ in intra-orbital channels. This suggests that multi-orbital degrees of freedom are crucial for realizing finite-momentum pairing. However, when the orbital nature is disregarded, the pairings in all the three IRs reduce to s-wave spin-singlet pairings. This implies that these pairings can arise through the proximity effect between an URM and a conventional SC. To illustrate this, we consider a planar URM-SC junction, as depicted in Fig. 3(a). At the interface, the proximity effect can be described by a mean-field Hamiltonian,

$$H_{prox} = H_{UR} + \sum_{\mathbf{k}, \sigma} \xi_{\mathbf{k}}^d d_{\mathbf{k}\sigma}^\dagger d_{\mathbf{k}\sigma} - \sum_{\mathbf{k}} \left(\Delta d_{\mathbf{k}\uparrow}^\dagger d_{-\mathbf{k}\downarrow}^\dagger + h.c. \right) + \frac{1}{2} \sum_{\mathbf{k}, \mathbf{q}, i, \sigma} \left(\mathbf{t}_i c_{\mathbf{k}+\frac{\mathbf{q}}{2}, i\sigma}^\dagger d_{\mathbf{k}\sigma} + h.c. \right). \quad (4)$$

Here, $d_{\mathbf{k}\sigma}^\dagger$ ($d_{\mathbf{k}\sigma}$) are the electron creation (annihilation) operators in the SC. $\xi_{\mathbf{k}}^d$ denotes the energy dispersion for the normal states of the SC, while Δ refers to the pairing order parameter. The second line describes the couplings between the URM and SC. For simplicity, we assume that the hopping integral $\mathbf{t}_{\mathbf{k}\mathbf{p}} \equiv \mathbf{t}_i$ are independent of \mathbf{k} and $\mathbf{p} \equiv \mathbf{k} + \mathbf{q}/2$. Additionally, we consider orbital-selective hopping integrals ($\mathbf{t}_1, \mathbf{t}_2$). Here, \mathbf{q} represents the center-of-mass momentum of the Cooper pairs, which is determined by the Cooper-pair propagator in each channel as they propagate into the URM. The coupling between the URM and SC mixes electrons and holes, revealing the nature of the induced order parameter in the URM. This interfacial pairing, induced by the proximity effect, can be derived using either the down-folding perturbation method or the Green-function equations of motion method [48]. Assuming a weak proximity effect ($|\mathbf{t}_{1/2}|/\Delta \ll 1$), we obtain three effective orbital-selective order parameters ($\Delta_{eff}^{1g1}(\mathbf{k}), \Delta_{eff}^{1g2}(\mathbf{k}), \Delta_{eff}^{1u}(\mathbf{k}) \propto -((\mathbf{t}_1^2 + \mathbf{t}_2^2), 2\mathbf{t}_1\mathbf{t}_2, (\mathbf{t}_1^2 - \mathbf{t}_2^2))/\Delta$).

Different interfacial pairings can be realized by tuning the hopping integrals. Specifically, we consider the case involves two orbitals of the URM, primarily derived from $d_{x^2-y^2}$ and d_{xy} orbitals. Orbital-selective proximity effects are realized by aligning the interface along either x or y axes, or along the diagonals $y = \pm x$, as shown in Fig. 3(a). This configuration results in $\mathbf{t}_1 \neq 0, \mathbf{t}_2 = 0$ or vice versa, causing the $1g2$ channel to vanish while the $1g1$ and $1u$ channels coexist.

The orbital-selective interfacial order parameters penetrate into the URM with a decay behavior. To describe the propagation of the order parameter, we introduce the

Cooper-pair propagator [14, 48, 57],

$$D_{\Gamma, \Gamma'}(1; 2) = -\langle T_\tau \hat{c}^T(1) \hat{\Gamma}^\dagger \hat{c}(1) \hat{c}^\dagger(2) \hat{\Gamma}' \hat{c}^*(2) \rangle. \quad (5)$$

Here, index $i \in \{1, 2\}$ labels real space coordinate $\mathbf{r}_i = (x_i, y_i)$ and imaginary time τ_i , that $\hat{c}^\dagger(i) \equiv \hat{c}^\dagger(\mathbf{r}_i, \tau_i) = (c_{1\uparrow}^\dagger(\mathbf{r}_i, \tau_i), c_{1\downarrow}^\dagger(\mathbf{r}_i, \tau_i), c_{2\uparrow}^\dagger(\mathbf{r}_i, \tau_i), c_{2\downarrow}^\dagger(\mathbf{r}_i, \tau_i))$. For convenience, we define $\mathbf{r} = \mathbf{r}_1 - \mathbf{r}_2$ and $\tau = \tau_1 - \tau_2$. Γ and Γ' stand for pairings in $\{1g1, 1g2, 1u\}$ in Table I. T_τ is the time ordering operator. After performing a Fourier transformation in imaginary time, the Cooper-pair propagator can be calculated [48].

The local order parameter inside the URM is phenomenologically derived from the propagators as,

$$\Delta_\Gamma(\mathbf{r}_1) = \sum_{\Gamma'} \lambda_{\Gamma'} \int_{-W/2}^{W/2} dx_2 D_{\Gamma, \Gamma'}(x_1, y_1; x_2, 0). \quad (6)$$

Here, the Cooper-pair propagator takes the retarded form $D_{\Gamma, \Gamma'}(\mathbf{r}_1; \mathbf{r}_2) \equiv D_{\Gamma, \Gamma'}(\mathbf{r}_1 - \mathbf{r}_2, \omega \rightarrow 0^+)$. $\lambda_{\Gamma'}$ is the strength of the order parameter for pairing form Γ' at the interface. Since the proximity effect is orbital selective with $\mathbf{t}_1 \neq 0$ and $\mathbf{t}_2 = 0$ as shown in Fig. 3(a), $\lambda_{\Gamma'}$ vanishes for the $1g2$ pairing, leaving only the $1g1$ and $1u$ pairings. The propagators for the $1g1$ and $1u$ channels are given by,

$$D_{1g1}(\mathbf{r}) = -1/2\pi^2 \gamma'_0 r^2, \quad (7)$$

$$D_{1u}(\mathbf{r}) = -\frac{g(+, -)}{4\pi^2 \gamma'_0 r^2} \eta \cos(q_0 r). \quad (8)$$

Here, $g(+, -) = 1 - \cos \phi_+ \cos \phi_- + \sin \phi_+ \sin \phi_-$, $\phi_\pm = \arctan[\lambda_R(D_0 \mp \varepsilon \lambda_R)/2\gamma'_0 \lambda]$, $\eta = \sqrt{(1 - \varepsilon^2 \frac{\lambda_R^2}{D_0^2})}$. Applying this to the SC-URM junction in Fig. 3(a), both $1g1$ and LO-type $1u$ pairings can be induced by the proximity effect. For a wide planar URM-SC junction, the induced order parameters become homogeneous along the interface and independent on the junction width W , i.e., $\Delta(\mathbf{r}_1) \approx \Delta(y_1) = \Delta(y)$. Combining with Eqs. (6), (7) and (8), we have

$$\Delta_{1g1}(y) = \varepsilon \Delta_0 / q_0 y, \quad (9)$$

$$\Delta_{1u}(y) = \varepsilon \Delta_0 \frac{g(+, -)}{\sqrt{2\pi}(q_0 y)^{3/2}} \eta \cos(q_0 y + \frac{\pi}{4}). \quad (10)$$

Here, $\Delta_0 = \lambda_0 \lambda_R / 2\pi \gamma'_0$ under the assumption of $\lambda_{1g1} = \lambda_{1u} = \lambda_0$. $\Delta_{1g1}(y)$ and $\Delta_{1u}(y)$ exhibit spatial decay proportional to y^{-1} and $y^{-3/2}$, respectively. Interestingly, $\Delta_{1u}(y)$ shows additional cosine oscillatory behavior, indicating a nonzero center-of-mass momentum q_0 , corresponding to the difference in the Fermi wave vectors between the inner and outer Fermi surfaces. Notably, $g(+, -) \sim \frac{1}{2}(\lambda_R D_0 / \gamma_0 \lambda)^2 \approx (\lambda_R k_F / \lambda)^2$, meaning the $1u$ pairing is suppressed when $\lambda_R k_F \ll \lambda$. This is consistent with our earlier microscopic results. In Fig. 3, we plot

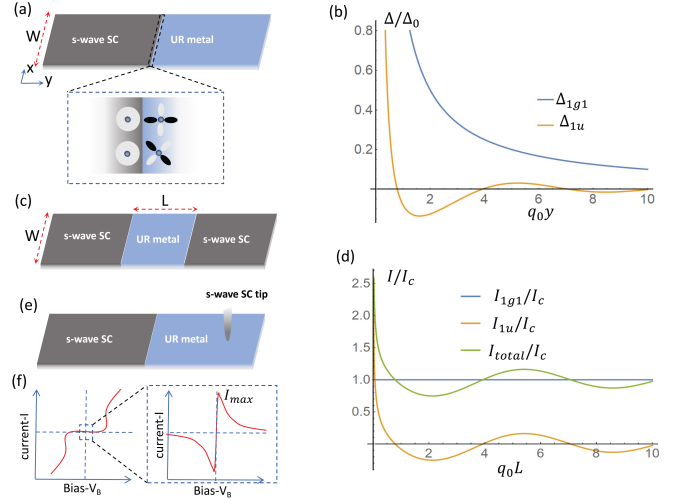


FIG. 3. (a) Schematic of a planar SC-URM junction. The zoom-in schematically illustrates the orbital selective proximity coupling between SC and URM at the interface. Here, we assume main s orbitals in SC and main $d_{x^2-y^2}$, d_{xy} orbitals in URM. (b) The two local orbital-selective-proximity-effect-induced order parameters in the URM as a function of $q_0 y$. (c) Schematic of a planar SC-URM-SC Josephson junction. The width in x -direction is W and the length of middle URM in y -direction is L . (d) The two individual and total critical currents as a function of $q_0 L$ in the planar SC-URM-SC Josephson junction. (e) Schematic of a JSTM/S platform to measure the tunneling current across the SC tip. (f) Schematic of typical $I - V_B$ relation from JSTM/S measurement shown in (e). The zoom-in schematically illustrates the $I - V_B$ relation near zero bias V_B .

$\Delta(0, y)$ as a function of dimensionless length $q_0 y$, clearly showing both the oscillation and decay behavior for $1u$ pairing.

Detection of LO-type pairing.— To detect the proximity-effect-induced LO-type pairing, one can exploit the Josephson effect [14, 58, 59]. To derive the current, we begin with the action for the URM under the proximity effect of the SC. In the real space and frequency domains, the action is given by,

$$S = - \sum_{i\omega_n} \int d^2 r_1 d^2 r_2 \hat{c}(\mathbf{r}_1; i\omega_n) \mathcal{G}^{-1}(\mathbf{r}; i\omega_n) \hat{c}(\mathbf{r}_2; i\omega_n) - \sum_{i\omega_n, \Gamma} \int d^2 r_1 \left[\Delta_\Gamma(\mathbf{r}_1) \hat{c}(\mathbf{r}_1; i\omega_n) \hat{\Gamma} \hat{c}^T(\mathbf{r}_1; -i\omega_n) + h.c. \right]. \quad (11)$$

Here, the spinor of Grassman numbers are $\hat{c} = (\bar{c}_{1\uparrow}, \bar{c}_{1\downarrow}, \bar{c}_{2\uparrow}, \bar{c}_{2\downarrow})$. $\mathcal{G}(\mathbf{r}; i\omega_n)$ is the relevant Matsubara Green function with the frequency $i\omega_n$ of fermions and integer n . [39]. Δ_Γ is the order parameter for $\hat{\Gamma} \in \{1g1, 1g2, 1u\}$. Integration of the electron field gives a

free energy in the second order of Δ_Γ .

$$F_2 = -2 \sum_{\Gamma, \Gamma'} \int d^2 r_1 d^2 r_2 \Delta_\Gamma(\mathbf{r}_2) \Delta_{\Gamma'}^*(\mathbf{r}_1) D_{\Gamma, \Gamma'}(\mathbf{r}_1; \mathbf{r}_2). \quad (12)$$

We consider a planar SC-URM-SC junction in the x - y plane to compute the Josephson current. The junction has length L in y -direction and width W in x -direction, as shown in Fig. 3(c). Considering a weak proximity effect, $\Delta_\Gamma(\mathbf{r})$ is nonzero only at the URM-SC interface, i.e., $\Delta_\Gamma = \Delta_{\Gamma, a} \delta(y) + \Delta_{\Gamma, b} \delta(y - L)$ with $\delta(y)$ a Delta function. Since the interfacial order parameters in different channels are induced by the same SC, they share the same phase $\Delta_{\Gamma, j} = \lambda_{\Gamma, j} e^{i\phi_j}$ with $j \in \{a, b\}$, and $\lambda_{\Gamma, j}$ is real. Due to the orbital-selective proximity effect, the cross terms $D_{\Gamma, \Gamma'}$ ($\Gamma \neq \Gamma'$) in Eq. (12) do not contribute. The Josephson current is given by $I = e/\hbar \partial F_2(\delta\phi)/\partial \delta\phi$, leading to $I = \sin(\delta\phi) \sum_\Gamma I_\Gamma$, where the critical current for each channel is given by

$$I_\Gamma = 4 \frac{e}{\hbar} \lambda_{\Gamma, a} \lambda_{\Gamma, b} \int_{-W/2}^{W/2} dx_1 dx_2 D_\Gamma(x_1, L; x_2, 0), \quad (13)$$

and $\delta\phi = \phi_a - \phi_b$. This result indicates that the Josephson critical current is determined by the propagation of Cooper pairs. Using Eqs. (7) and (8), we obtain

$$I_{1g1} \equiv I_c = 2(w/l) e \lambda_a \lambda_b / \pi \gamma_0' \hbar, \quad (14)$$

$$I_{1u} = \frac{g(+, -)}{\sqrt{2\pi l}} I_c \eta \cos\left(l + \frac{\pi}{4}\right). \quad (15)$$

Here, we define the dimensionless quantities $l = q_0 L$, $w = q_0 W$. The critical current of $1u$ channel in Eq. (15) inherits spatial oscillations from the propagator, indicating that positive, negative or zero currents can occur by varying the length L of the URM or by introducing dopings to change q_0 in the junction as the decay behavior is renormalized. The renormalized critical currents for individual and total channels are shown in Fig. 3(d).

In experiments, JSTM/S provides an alternative method to detect LO-type pairing [60, 61]. In the setup shown in Fig. 3(e), the local critical current can be computed using Eq. (13) with replacing $\int dx_1 dx_2 \rightarrow \int dx_1 dx_2 \delta(x_1)$ and $L \rightarrow y$ under the conditions of large width W and negligible contributions from reflected Cooper pairs. The schematic of local $I - V_B$ relation is shown in Fig. 3(f). The maximum current $I_{max}(y)$ across the SC tip at a finite bias is proportional to $[I_{1g1}(y) + I_{1u}(y)]^2$ [60–63]. Thus, the current $I_{max}(y)$ should exhibit a strip pattern with a spatial period of $2\pi/q_0$, as renormalized by the coexistence of the trivial $1g1$ channel, similar to Fig. 3(d).

Conclusion.— In summary, we demonstrate that both intrinsic and extrinsic finite-momentum pairings can be generated in unconventional Rashba systems, driven by microscopic interactions and the superconducting proximity effect, respectively. In both cases, the internal

multi-orbital structure plays a crucial role. An unexpected and significant result is that the coexistence of both zero-momentum and LO-type pairings in different channels offers valuable insights into experimentally observed PDW states. We also propose two methods for detecting the LO-type pairing induced by the proximity effect. This investigation provides a deeper understanding of the rich and complex behavior of finite-momentum pairings in superconductors, particularly in multi-orbital systems.

This work was financially supported by the National Key R&D Program of China (Grants No. 2022YFA1403200), National Natural Science Foundation of China (Grants No. 92265104, No. 12022413), the Basic Research Program of the Chinese Academy of Sciences Based on Major Scientific Infrastructures (Grant No. JZHKYPT-2021-08), the CASHIPS Director's Fund (Grant No. BJPY2023A09), the ‘‘Strategic Priority Research Program (B)’’ of the Chinese Academy of Sciences (Grant No. XDB33030100), Anhui Provincial Major S&T Project(s202305a12020005) and the Major Basic Program of Natural Science Foundation of Shandong Province (Grant No. ZR2021ZD01), and the High Magnetic Field Laboratory of Anhui Province under Contract No. AHM-FX-2020-02. S.B.Z acknowledges the start-up fund at HFNL, the Innovation Program for Quantum Science and Technology (Grant No. 2021ZD0302800), and Anhui Initiative in Quantum Information Technologies (Grant No. AHY170000).

* haon@hmf.ac.cn

- [1] R. Casalbuoni and G. Nardulli, Inhomogeneous superconductivity in condensed matter and qcd, *Reviews of Modern Physics* **76**, 263 (2004).
- [2] D. F. Agterberg, J. S. Davis, S. D. Edkins, E. Fradkin, D. J. Van Harlingen, S. A. Kivelson, P. A. Lee, L. Radzihovsky, J. M. Tranquada, and Y. Wang, The physics of pair-density waves: Cuprate superconductors and beyond, *Annual Review of Condensed Matter Physics* **11**, 231 (2020).
- [3] P. Fulde and R. A. Ferrell, Superconductivity in a strong spin-exchange field, *Phys. Rev.* **135**, A550 (1964).
- [4] A. I. Larkin and Y. N. Ovchinnikov, Nonuniform state of superconductors, *Zh. Eksp. Teor. Fiz.* 47, 1136 (1964) [*Sov. Phys. JETP* 20, 762 (1965)] (1964).
- [5] J. J. Kinnunen, J. E. Baarsma, J.-P. Martikainen, and P. Törmä, The fulde–ferrell–larkin–ovchinnikov state for ultracold fermions in lattice and harmonic potentials: a review, *Reports on Progress in Physics* **81**, 046401 (2018).
- [6] D. F. Agterberg and H. Tsunetsugu, Dislocations and vortices in pair-density-wave superconductors, *Nature Physics* **4**, 639 (2008).
- [7] E. Berg, E. Fradkin, and S. A. Kivelson, Theory of the striped superconductor, *Phys. Rev. B* **79**, 064515 (2009).
- [8] F. Loder, A. P. Kampf, and T. Kopp, Superconducting

- state with a finite-momentum pairing mechanism in zero external magnetic field, *Phys. Rev. B* **81**, 020511 (2010).
- [9] R. Soto-Garrido and E. Fradkin, Pair-density-wave superconducting states and electronic liquid-crystal phases, *Phys. Rev. B* **89**, 165126 (2014).
- [10] E. Berg, E. Fradkin, E.-A. Kim, S. A. Kivelson, V. Oganesyan, J. M. Tranquada, and S. C. Zhang, Dynamical layer decoupling in a stripe-ordered high- T_c superconductor, *Phys. Rev. Lett.* **99**, 127003 (2007).
- [11] P. A. Lee, Amperian pairing and the pseudogap phase of cuprate superconductors, *Physical Review X* **4**, 031017 (2014).
- [12] E. Berg, E. Fradkin, and S. A. Kivelson, Charge-4 e superconductivity from pair-density-wave order in certain high-temperature superconductors, *Nature Physics* **5**, 830 (2009).
- [13] Y. Wang, S. D. Edkins, M. H. Hamidian, J. S. Davis, E. Fradkin, and S. A. Kivelson, Pair density waves in superconducting vortex halos, *Physical Review B* **97**, 174510 (2018).
- [14] S.-B. Zhang, L.-H. Hu, and T. Neupert, Finite-momentum cooper pairing in proximitized altermagnets, *Nature Communications* **15**, 10.1038/s41467-024-45951-3 (2024).
- [15] D. Chakraborty and A. M. Black-Schaffer, Zero-field finite-momentum and field-induced superconductivity in altermagnets, *Phys. Rev. B* **110**, L060508 (2024).
- [16] G. Sim and J. Knolle, Pair density waves and supercurrent diode effect in altermagnets, arXiv preprint [arXiv:2407.01513](https://arxiv.org/abs/2407.01513) (2024).
- [17] D. Chakraborty and A. M. Black-Schaffer, Perfect superconducting diode effect in altermagnets, arXiv preprint [arXiv:2408.07747](https://arxiv.org/abs/2408.07747) (2024).
- [18] Z.-T. Sun, R.-P. Yu, S. A. Chen, J.-X. Hu, and K. T. Law, Flat-band fulde-ferrell-larkin-ovchinnikov state from quantum geometry discrepancy, arXiv preprint [arXiv:2408.00548](https://arxiv.org/abs/2408.00548) (2024).
- [19] S. Takada, Superconductivity in a molecular field. ii: Stability of fulde-ferrel phase, *Progress of Theoretical Physics* **43**, 27 (1970).
- [20] Q. Wang, C.-R. Hu, and C.-S. Ting, Impurity-induced configuration-transition in the fulde-ferrell-larkin-ovchinnikov state of a d -wave superconductor, *Phys. Rev. B* **75**, 184515 (2007).
- [21] L. W. Gruenberg and L. Gunther, Fulde-ferrell effect in type-ii superconductors, *Phys. Rev. Lett.* **16**, 996 (1966).
- [22] H. Adachi and R. Ikeda, Effects of pauli paramagnetism on the superconducting vortex phase diagram in strong fields, *Phys. Rev. B* **68**, 184510 (2003).
- [23] W. Chen and W. Huang, Pair density wave facilitated by bloch quantum geometry in nearly flat band multi-orbital superconductors, *Science China Physics, Mechanics & Astronomy* **66**, 287212 (2023).
- [24] G. Jiang and Y. Barlas, Pair density waves from local band geometry, *Physical Review Letters* **131**, 016002 (2023).
- [25] H.-X. Wang and W. Huang, Quantum-geometry-facilitated pair density wave order: Density matrix renormalization group study, arXiv preprint [arXiv:2406.17187](https://arxiv.org/abs/2406.17187) (2024).
- [26] H.-D. Chen, O. Vafek, A. Yazdani, and S.-C. Zhang, Pair density wave in the pseudogap state of high temperature superconductors, *Phys. Rev. Lett.* **93**, 187002 (2004).
- [27] D. F. Agterberg and R. P. Kaur, Magnetic-field-induced helical and stripe phases in rashba superconductors, *Phys. Rev. B* **75**, 064511 (2007).
- [28] O. Dimitrova and M. V. Feigel'man, Theory of a two-dimensional superconductor with broken inversion symmetry, *Phys. Rev. B* **76**, 014522 (2007).
- [29] N. F. Q. Yuan and L. Fu, Topological metals and finite-momentum superconductors, *Proc Natl Acad Sci U S A* **118** (2021).
- [30] N. F. Q. Yuan and L. Fu, Supercurrent diode effect and finite-momentum superconductors, *Proc Natl Acad Sci U S A* **119**, e2119548119 (2022).
- [31] E. I. Rashba, Properties of semiconductors with an extremum loop .i. cyclotron and combinational resonance in a magnetic field perpendicular to the plane of the loop, *Sov. Phys. Solid. State* **2**, 1109 (1960).
- [32] Y. A. Bychkov and E. I. Rashba, Properties of a 2d electron-gas with lifted spectral degeneracy, *Jetp Letters* **39**, 78 (1984).
- [33] R. Winkler and U. Rössler, General approach to the envelope-function approximation based on a quadrature method, *Phys. Rev. B* **48**, 8918 (1993).
- [34] R. Winkler, Rashba spin splitting in two-dimensional electron and hole systems, *Phys. Rev. B* **62**, 4245 (2000).
- [35] L. P. Gor'kov and E. I. Rashba, Superconducting 2d system with lifted spin degeneracy: Mixed singlet-triplet state, *Phys. Rev. Lett.* **87**, 037004 (2001).
- [36] P. A. Frigeri, D. F. Agterberg, A. Koga, and M. Sigrist, Superconductivity without inversion symmetry: MnSi versus CePt_3Si , *Phys. Rev. Lett.* **92**, 097001 (2004).
- [37] X. Huang, Y. Xiao, R. Song, and N. Hao, Generic model with unconventional rashba bands and giant spin galvanic effect, *Phys. Rev. B* **109**, 195419 (2024).
- [38] R. Song, N. Hao, and P. Zhang, Giant inverse rashba-edelstein effect: Application to monolayer osbi 2, *Physical Review B* **104**, 115433 (2021).
- [39] R. Wang, J. Li, X. Huang, L. Wang, R. Song, and N. Hao, Superconductivity in two-dimensional systems with unconventional rashba bands, *Phys. Rev. B* **110**, 134517 (2024).
- [40] A. Bhattacharya and A. M. Black-Schaffer, Electric field induced second-order anomalous hall transport in unconventional rashba system, arXiv: 2408.15840 (2024).
- [41] W. Gao, X. Zhu, F. Zheng, M. Wu, J. Zhang, C. Xi, P. Zhang, Y. Zhang, N. Hao, W. Ning, *et al.*, A possible candidate for triply degenerate point fermions in trigonal layered ptbi2, *Nature communications* **9**, 3249 (2018).
- [42] G. E. V. Gor'kov and L. P., An unusual superconductivity in ube13, *JETP* (1984).
- [43] G. E. V. Gor'kov and L. P., Superconducting classes in heavy-fermion systems, *Soviet Physics JETP* (1985).
- [44] K. Ueda and T. M. Rice, P-wave superconductivity in cubic metals, *Physical Review B* **31**, 7114 (1985).
- [45] M. Sigrist and K. Ueda, Phenomenological theory of unconventional superconductivity, *Rev. Mod. Phys.* **63**, 239 (1991).
- [46] C. Wen, X. Zhu, Z. Xiao, N. Hao, R. Mondaini, H. Guo, and S. Feng, Superconducting pairing symmetry in the kagome-lattice hubbard model, *Physical Review B* **105**, 075118 (2022).
- [47] W. Yang, C.-J. Mo, S.-B. Fu, Y. Yang, F.-W. Zheng, X.-H. Wang, Y.-A. Liu, N. Hao, and P. Zhang, Soft-mode-phonon-mediated unconventional superconductivity in monolayer $1\text{t}'\text{-wte 2}$, *Physical Review Letters* **125**, 237006 (2020).

- [48] Supplementary material, .
- [49] D. E. Sheehy and L. Radzihovsky, Bc-bcs crossover in “magnetized” feshbach-resonantly paired superfluids, *Phys. Rev. Lett.* **96**, 060401 (2006).
- [50] D. E. Sheehy and L. Radzihovsky, Bc-bcs crossover, phase transitions and phase separation in polarized resonantly-paired superfluids, *Annals of Physics* **322**, 1790 (2007).
- [51] Y. Liu, T. Wei, G. He, Y. Zhang, Z. Wang, and J. Wang, Pair density wave state in a monolayer high-t c iron-based superconductor, *Nature* **618**, 934 (2023).
- [52] H. Zhao, R. Blackwell, M. Thinel, T. Handa, S. Ishida, X. Zhu, A. Iyo, H. Eisaki, A. N. Pasupathy, and K. Fujita, Smectic pair-density-wave order in eurbfe4as4, *Nature* **618**, 940 (2023).
- [53] T. Wei, Y. Liu, W. Ren, Z. Wang, and J. Wang, Observation of intra-unit-cell superconductivity modulation, arXiv preprint [arXiv:2404.16683](https://arxiv.org/abs/2404.16683) (2024).
- [54] L. Kong, M. Papaj, H. Kim, Y. Zhang, E. Baum, H. Li, K. Watanabe, T. Taniguchi, G. Gu, P. A. Lee, *et al.*, Observation of cooper-pair density modulation state, arXiv preprint [arXiv:2404.10046](https://arxiv.org/abs/2404.10046) (2024).
- [55] Y. Zhang, L. Yang, C. Liu, W. Zhang, and Y.-S. Fu, Visualizing uniform lattice-scale pair density wave in single-layer fese/srtio3 films, arXiv preprint [arXiv:2406.05693](https://arxiv.org/abs/2406.05693) (2024).
- [56] Q. Gu, J. P. Carroll, S. Wang, S. Ran, C. Broyles, H. Sidiquee, N. P. Butch, S. R. Saha, J. Paglione, J. S. Davis, *et al.*, Detection of a pair density wave state in ute2, *Nature* **618**, 921 (2023).
- [57] P. A. Lee and M. G. Payne, Pair propagator approach to fluctuation-induced diamagnetism in superconductors-effects of impurities, *Phys. Rev. B* **5**, 923 (1972).
- [58] S. Hart, H. Ren, M. Kosowsky, G. Ben-Shach, P. Leubner, C. Brüne, H. Buhmann, L. W. Molenkamp, B. I. Halperin, and A. Yacoby, Controlled finite momentum pairing and spatially varying order parameter in proximitized hgte quantum wells, *Nature Physics* **13**, 87 (2017).
- [59] A. Q. Chen, M. J. Park, S. T. Gill, Y. Xiao, D. Reig-i Plessis, G. J. MacDougall, M. J. Gilbert, and N. Mason, Finite momentum cooper pairing in three-dimensional topological insulator josephson junctions, *Nature Communications* **9**, [10.1038/s41467-018-05993-w](https://doi.org/10.1038/s41467-018-05993-w) (2018).
- [60] M. Hamidian, S. D. Edkins, S. H. Joo, A. Kostin, H. Eisaki, S. Uchida, M. Lawler, E.-A. Kim, A. P. Mackenzie, K. Fujita, *et al.*, Detection of a cooper-pair density wave in bi2sr2cacu2o8+ x, *Nature* **532**, 343 (2016).
- [61] D. Cho, K. Bastiaans, D. Chatzopoulos, G. Gu, and M. Allan, A strongly inhomogeneous superfluid in an iron-based superconductor, *Nature* **571**, 541 (2019).
- [62] Y. Anchenko and L. Zil’berman, The josephson effect in small tunnel contacts, *Soviet Phys. JETP* **28** (1969).
- [63] G.-L. Ingold, H. Grabert, and U. Eberhardt, Cooper-pair current through ultrasmall josephson junctions, *Physical Review B* **50**, 395 (1994).